ACS OMEGA

Open Access

http://pubs.acs.org/journal/acsodf

Article

Investigating the Protein-Based Therapeutic Relationship between Honey Protein SHP-60 and Bevacizumab on Angiogenesis: Exploring the Synergistic Effect through In Vitro and In Silico Analysis

Mohsin Wahid,* Meshal Nazeer, Abdul Qadir, and Muhammad Bilal Azmi

Cite This: *ACS Omega* 2024, 9, 17143−17153

Read Online

ACCESS | Metrics & More | Article Recommendations

ABSTRACT: Honey is a natural product produced by honeybees, which has been used not only as food but also as a medicine by humans for thousands of years. In this study, 60 kDa protein was purified from Pakistani Sidr honey named as SHP-60 (Sidr Honey Protein-60), and its antioxidant potential and the effect of Bevacizumab with purified protein on in vitro angiogenesis using human umbilical vein endothelial cells (HUVEC) were investigated. We further validated the molecular protein−protein (SHP-60 with Bevacizumab) interactions through in silico analysis. It showed very promising antioxidant activity by reducing 2,2-diphenyl-1-picrylhydrazyl free radicals with a maximum of 83% inhibition at 50 μM and an IC_{50} of 26.45 μM statistically significant (**$p < 0.01$). Angiogenesis is considered a hallmark of cancer, and without it, the tumor cannot grow or metastasize. Bevacizumab, SHP-60, and both in combination were used to treat HUVEC, and the MTT assay was used to assess cell viability. To demonstrate in vitro angiogenesis, HUVEC was grown on Geltrex, and the formation of endotubes was examined using a tube formation assay. HUVEC viability was dose-dependently decreased by Bevacizumab, SHP-60, and both together. Bevacizumab and SHP-60 both inhibited angiogenesis in vitro, and their combination displayed levels of inhibition even higher than those of Bevacizumab alone. We investigated the protein−protein molecular docking interactions and molecular dynamics simulation analysis of MRJP3 (major royal jelly protein 3) similar to SHP-60 in molecular weight with both the heavy chain (HC) and light chain (LC) of Bevacizumab. We found significant interactions between the LC and MRJP3, indicating that ASN468, GLN470, and ASN473 of MRJP3 interact with SER156, SER159, and GLU161 of LC of Bevacizumab. The integration of experimental data and computational techniques is believed to improve the reliability of the findings and aid in future drug design.

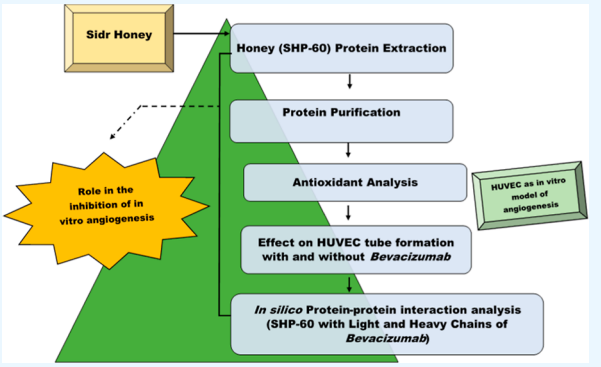

1. INTRODUCTION

Cancer is considered as a leading cause of death all over the world, and its treatment is still a major challenge in the field of medicine. Cancer development has both genetics and environmental factors involved and cancer prevention and risk has always been linked with diet and lifestyle modifications.[1] More recently, there has been a growing interest to investigate, at the molecular level, the role of natural products as chemotherapeutic and chemoprotective agents and examining their potential in targeting the hall marks of cancer including angiogenesis.[2] Honey has been shown to be a source of bioactive compounds and many medicinal properties of honey have been documented by modern research, which includes, anticancer, antibacterial, antidiabetic, antioxidant, antilipidemic, antiviral, and antigiardial bioactivities[3−5] The honey defense system has not only been reported against pathogens but also shows promising results against nematodes. The protozoan *Giardia lamblia* is the most common human parasite and causes diarrhea and malabsorption. Purified Ziziphus honey proteins were found to be very active against *G. lamblia*, with $IC_{50} \leq 25$ mg/mL[6]

The inhibition of tumor angiogenesis can have therapeutic implications as pathological angiogenesis occurs in chronic inflammatory diseases and tumors.[7] In pathological conditions, it not only provides nutrients and oxygen, which are essential for tumor growth, but also helps tumor cells enter the general circulation.[8] Endothelial cells produce the glycoprotein known as vascular endothelial growth factor (VEGF), which is one of the most important signaling molecules in charge of controlling angiogenesis. Cellular response is initiated when VEGF binds to its receptors.[9] Among all members, VEGF-A is mostly

Received: December 9, 2023
Revised: February 9, 2024
Accepted: March 11, 2024
Published: April 3, 2024

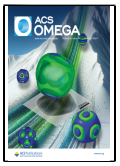

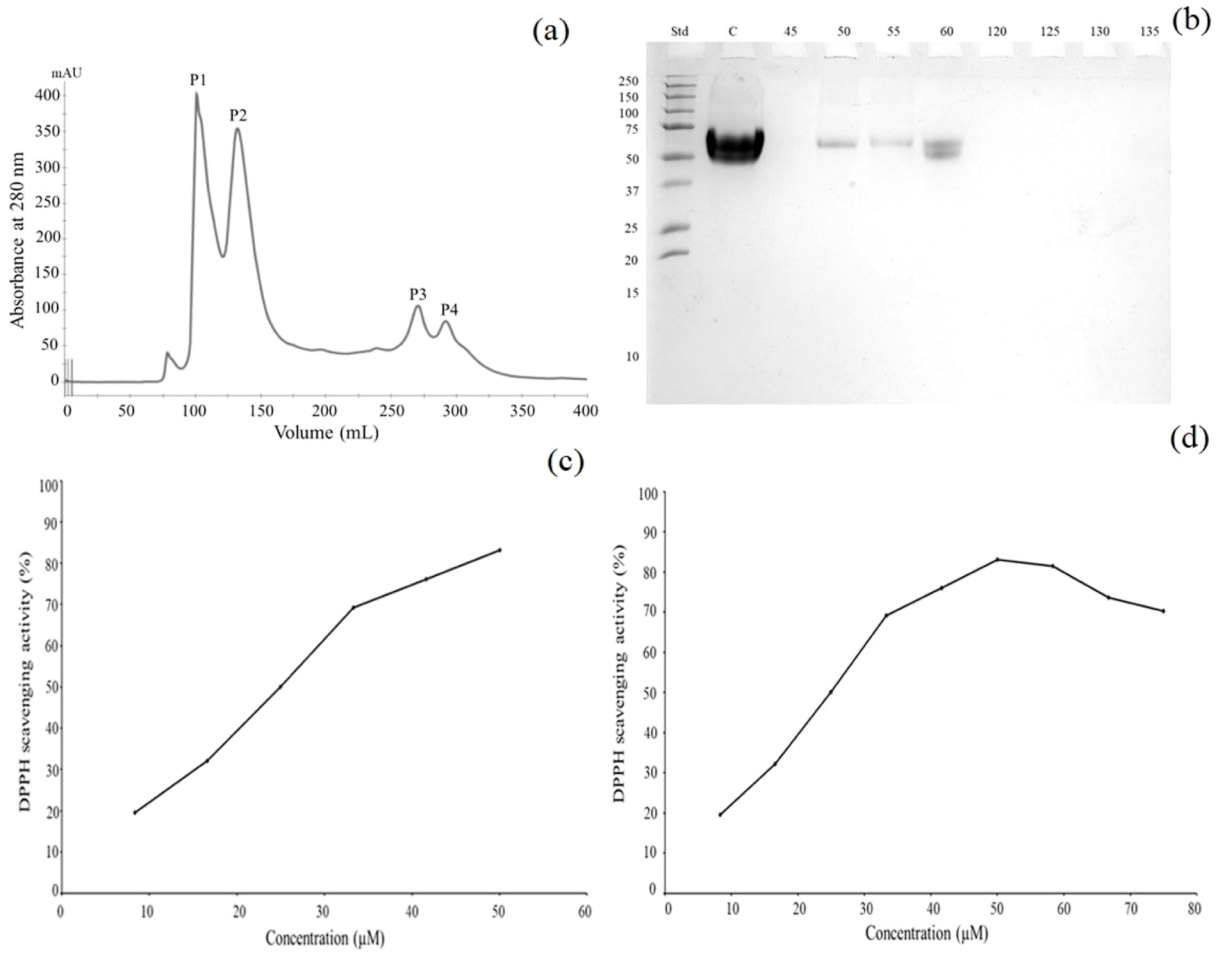

Figure 1. (a) Fractionation profile of Sidr honey crude proteins on Sephacryl S-200 (2.6 cm × 60 cm) column by FPLC. The chromatogram showed four peaks as P1, P2, P3, and P4. (b) Electrophoretic profile by Tris/Tricine SDS−PAGE (12%) of Sider honey crude proteins precipitates as C, and gel filtration chromatography fractions (45, 50, 55, 60, 120, 125, 130, and 135). Std, is standard molecular weight marker. (c) The graphical presentation of DPPH radicals scavenging activity of SHP-60 at different concentrations (μM). The level of significance is $^{**}P < 0.01$. (d) The hyperbolic presentation of DPPH radicals scavenging activity of purified SHP-60 at different concentrations (μM).

expressed in human cancers (colon, breast, head, lung, and neck), and it actively participates in tumor angiogenesis. Therefore, the inhibition of tumor angiogenesis by cancer treatment is currently an area of research that requires investigations at the molecular level and considered an ideal cancer combating strategy.[10] Bevacizumab is a monoclonal antibody (149 kDa) that is specific for VEGF. It binds with a high affinity to VEGF-A isoforms and inhibits angiogenesis by blocking VEGF-A from interacting with its receptors (VEGFR-1 and VEGFR-2). It is primarily used to treat colorectal cancer, renal cell carcinoma, and glioblastoma and has FDA (US Food and Drug Administration) approval. It is also used off-label to treat diabetic retinopathy, age-related macular degeneration, and iris neovascularization.[11]

A human umbilical vein endothelial cell (HUVEC) line is frequently used for in vitro investigations of endothelial cell (EC) function and in vitro angiogenesis.[12] The in vitro assays used for angiogenesis can investigate the effects on ECs migration, proliferation, apoptosis, and tube formation.

In the past two decades, many proteins from different honey samples have been reported to be biologically active components.[13,14] The overall protein content in honey is only 0.1 to 0.5%, and that is why we knew very less proteome content.[15,16] In this study, we focused on the least known proteome content of Sidr honey from Pakistan and purified 60 kDa protein named SHP-60 (Sidr Honey Protein-60). This honey was collected from the Karak district of KPK (Khyber Pakhtunkhwa), Pakistan. This is the first time the proteins from this species of honey have been explored. SHP-60 protein was purified using different techniques and then subjected to antioxidant and tumor angiogenesis investigations. Using HUVEC as an in vitro model, we examined the effects of bevacizumab and SHP-60 alone and in combination on tumor angiogenesis.

In this context, the current study's goal was to evaluate the antioxidant potential and tumor angiogenesis activity of purified SHP-60 from Sidr honey. To further evaluate the possible interaction of Bevacizumab with the SHP-60 which made tumor angiogenesis very promising, we performed in silico studies. For this purpose, we searched the honey proteins which are close to our SHP-60 in molecular weight by using UniProtKb reference protein database (https://www.uniprot.org/).[17] The major proteins found in honey are known as royal jelly (RJ) proteins, which includes almost nine members with molecular weights ranging from 49 to 87 kDa. These RJ proteins are also known as apalbumins (apa). The apalbumin1 (apa1), apalbumin2 (apa2), and apalbumin3 (apa3) account for major RJ protein content, with identical amino acid

https://doi.org/10.1021/acsomega.3c09736
ACS Omega 2024, 9, 17143−17153

sequences of almost 72%. These apa 1−3 proteins are very well documented as anticancer in vitro.[18,19] With this knowledge, we searched honey proteins similar in molecular weight to SHP-60 on UniProtKb, whose sequence is available. On different computational parameters we selected MRJP3,[20] and use this protein sequence as homology of SHP-60, to investigated the possible protein−protein interaction. Through in silico investigation, this protein−protein (MRJP3 with Bevacizumab) interaction's molecular binding pattern (synergistic effects) can be explored for regulating the angiogenesis challenge. Hence, the rationale of the study was to isolate and purify proteins from Pakistani Sidr honey and study its effect on inhibition of in vitro angiogenesis and in silico analysis to explore the protein-based interactions that can have any significant therapeutic implications. To the best of our knowledge, this is the first study that has purified protein from Pakistani Sidr honey and investigated its role on the inhibition of in vitro angiogenesis using HUVEC as a model.

2. RESULTS AND DISCUSSION

2.1. Purification of SPH-60 from Sidr Honey. The crude proteins from Sidr honey were extracted and then precipitated with 85% ammonium sulfate. The proteins were separated according to their molecular weight by FPLC using a gel filtration column. The gel filtration column Hi-prep 26/60 Sephacryl S-200, was equilibrated with buffer A. The elution profile (Figure 1a) indicated that proteins were segregated according to their molecular weights, and indicated four peaks as P1, P2, P3, and P4. The sodium dodecyl sulfate−polyacrylamide gel electrophoresis (SDS−PAGE) profile of crude as well as separated proteins by FPLC were achieved by 10% Tris/Tricine gel (Figure 2b), which clearly indicated that fraction numbers 50, and 55 have a single band of 60 kDa protein (SHP-60).

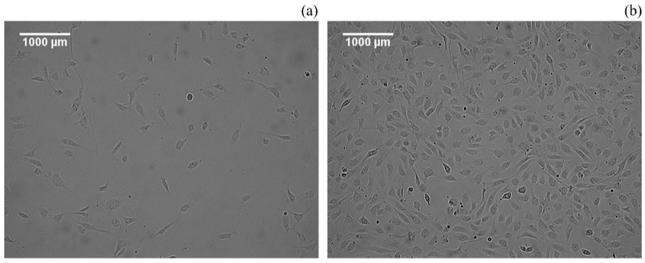

Figure 2. Morphology of the HUVEC. (a) The appearance of cells after 24 h of isolation. (b) Initially, there were few cells and then they started to proliferate and achieved 80% confluency by day 7. Image taken at 10× magnification (n = 3).

In previous studies, several proteins and peptides from different honeys have been isolated and evaluated as a bioactive entity. The protein having an approximate molecular weight of 261 was purified from the jungle honey (JH) of Nigeria and was found to have potent antitumor activity.[21] A 5.8 kDa component from Manuka honey was found to be involved in the stimulation of TNF-α via TLR4 (toll-like receptor 4).[22] The royal jelly protein of 55 kDa (apalbumin-1) was collected from honey and was found to be involved in the release of TNF-α from the macrophages of mouse.[19] Major royal jelly protein 1 (MRJP1), having a molecular weight of 55 kDa, was found to be active in wound healing of human keratinocytes by elevating the levels of cytokines (TGF-β, TNF- α, and IL-1β), and matrix metalloproteinase-9 (MMP-9).[23] Apisimin is a 5.6 kDa honeybee-derived protein from honey of New Zealand, which is known to be involved in TNF-α release from blood monocytes.[24] The kanuka honey (New Zealand) was found to be a stimulant for the release of TNF- α from U937, and THP-1 monocytic cell lines; this activity is associated with the type II arabinogalactan proteins (AGPs) with molecular weight >30 kDa.[25] All of these data showed the variation in the protein profile of different honey samples throughout the world. Every honey is unique by its proteins, and peptides components which depends on several factors (species of bees, geographical area, season, and environmental influences).[2,26] The fractions having purified 60 kDa protein (Figure 1b) were pooled together, freeze-dried, and then subjected to antioxidant potential and invitro angiogenesis.

2.2. 2,2-Diphenyl-1-Picrylhydrazyl Radicals Scavenging Activity. The results of 2,2-diphenyl-1-picrylhydrazyl (DPPH) radicals scavenging activity for Sidr honey purified protein SHP-60 are shown in Figure 1c,d. The results clearly indicated that SHP-60 exhibited promising antioxidant activity against DPPH. The calculated IC_{50} value was 26.45 μM which was statistically significant (**P < 0.01) (Figure 1c). The antioxidant activity of SHP-60 has been increased with increasing concentration (Figure 1c), and then, after maximum, it slowly drops down in a hyperbolic relationship (Figure 1d). The maximum activity was observed 83% at 50 μM concentration, and when protein concentration was increased further, the antioxidant activity was not increased rather it relatively slow down. At higher concentration SHP-60 may create saturation for antioxidant reaction which indirectly increased the phenomena of mass transfer limitation.[27] Every honey is different because of species of bees, geographical area, season, and environmental factors, which make every honey unique in its components.[26,28] In one study, different Algerian crude honeys were tested for antioxidant properties, and it was concluded that these honeys were found to be active antioxidants with average 39.7% DPPH radical scavenging ability at concentration 120 mg/mL.[29] In another study, Acacia, Gelam, and Tualang honey proteins were subjected for antioxidant activity by using DPPH, and these honey proteins were found to be active antioxidants. In the honey protein concentrations found to be very low typically 0.1 to 0.5%.[27] In our study, we used Sidr honey and purified 60 kDa (SHP-60) by FPLC, which was subjected to antioxidant activity. It showed that SHP-60 exhibited promising antioxidant activity. The minimum percentage inhibition of scavenging activity of SHP-60 for DPPH was observed to be 19.48%, at 8.33 μM, whereas the maximum percent inhibition was observed to be 83% at 50 μM concentration. The calculated IC_{50} value was 26.45 μM which was statistically significant (**P < 0.01). The IC_{50} value was calculated from the plotted graphs of scavenging activity against various concentrations of pure SHP-60. After maximum inhibition activity of SHP-60, when further increased in concentration, there was a decline observed in the inhibition of DPPH radicals hyperbolically (Figure 1d).

2.3. HUVEC Culture. HUVEC was thawed from −80 °C and plated in cell culture flasks. The next day, as observed under phase contrast microscopy, the cells were seen as attached to the base of T-75 flask within 24 h and started forming clusters. The cells achieved 80% confluence and displayed characteristic cobblestone morphology after 5−7 days using a phase contrast microscope (Figure 2).

https://doi.org/10.1021/acsomega.3c09736
ACS Omega 2024, 9, 17143−17153

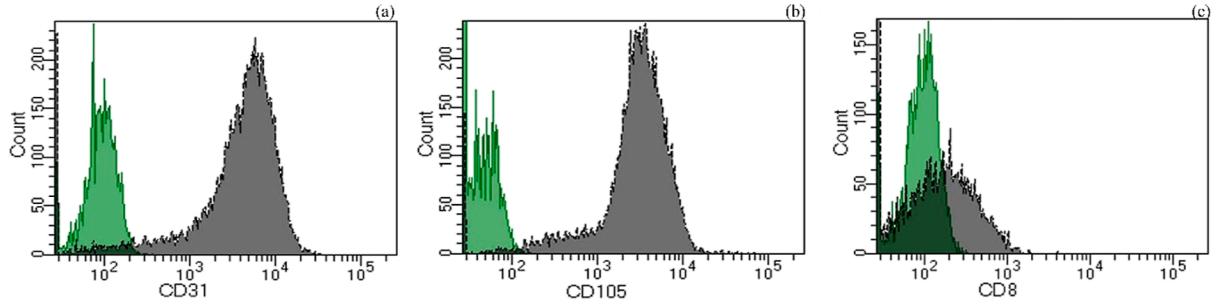

Figure 3. HUVEC characterization by flowcytometry. The flowcytometry analysis showed that HUVEC were positive for (a) CD31, (b) CD105, and negative for (c) CD8. The unstained control is illustrated in green, and the test sample is illustrated in gray (n = 3).

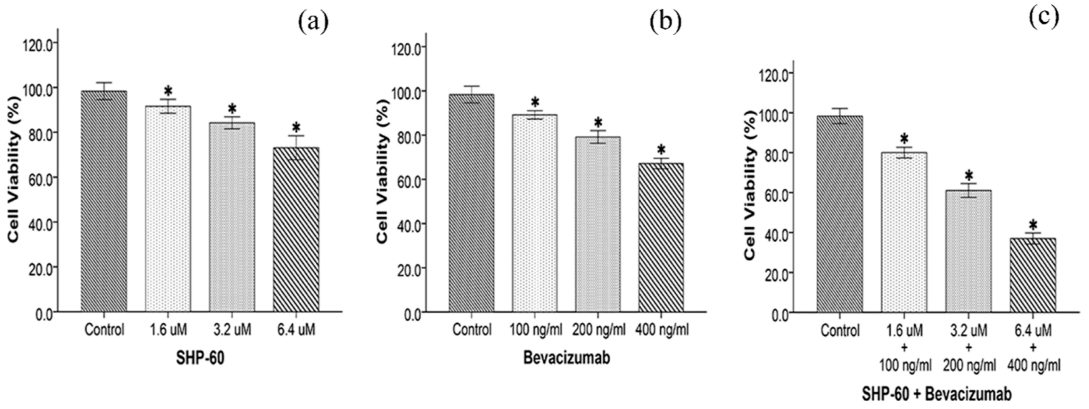

Figure 4. HUVEC viability. The figure shows the effect of (a) SHP-60, (b) Bevacizumab, and (c) the combination of both on HUVEC viability using the MTT assay. Each bar represents the mean ± SD of three independent experiments. *p < 0.05 as compared to control (n = 3).

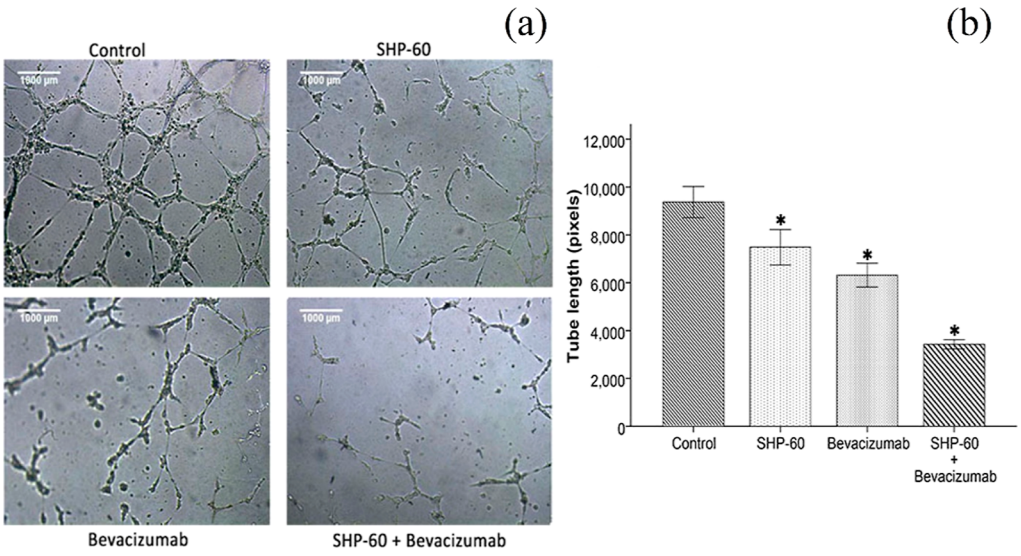

Figure 5. HUVEC tube formation. Figure (a) shows the effect of SHP-60, Bevacizumab, and their combination on HUVEC tube formation as compared to the control. Image taken at 10× magnification under the phase contrast microscope. Figure (b) shows the analysis of HUVEC tube formation. Each bar represents the mean ± SD of three independent experiments. *p < 0.05 as compared to control (n = 3).

2.4. Characterization of HUVEC by Flowcytometry. The results of flowcytometry indicated that HUVEC were positive for CD31 and CD105 and negative for CD8 antibodies (Figure 3). Endothelial cells have shown to express specific markers and their characterization at either mRNA or protein level was required so that it is confirmed that we are testing our downstream experiments on endothelial cells (HUVEC) which has already been shown to be a model of in vitro angiogenesis.[30−32] As shown previously, CD 31 is considered as an important marker for endothelial cells, and its protein expression in these HUVEC was shown by flowcytometry analysis. As shown in Figure 3, a very high percentage of cells showed expression of CD31 and CD105 in these HUVEC and showed no expression of CD 8 which was used as a negative marker as HUVEC do not express this marker. The results of flowcytometry validated that we are working with the cells that have been characterized using

https://doi.org/10.1021/acsomega.3c09736
ACS Omega 2024, 9, 17143−17153

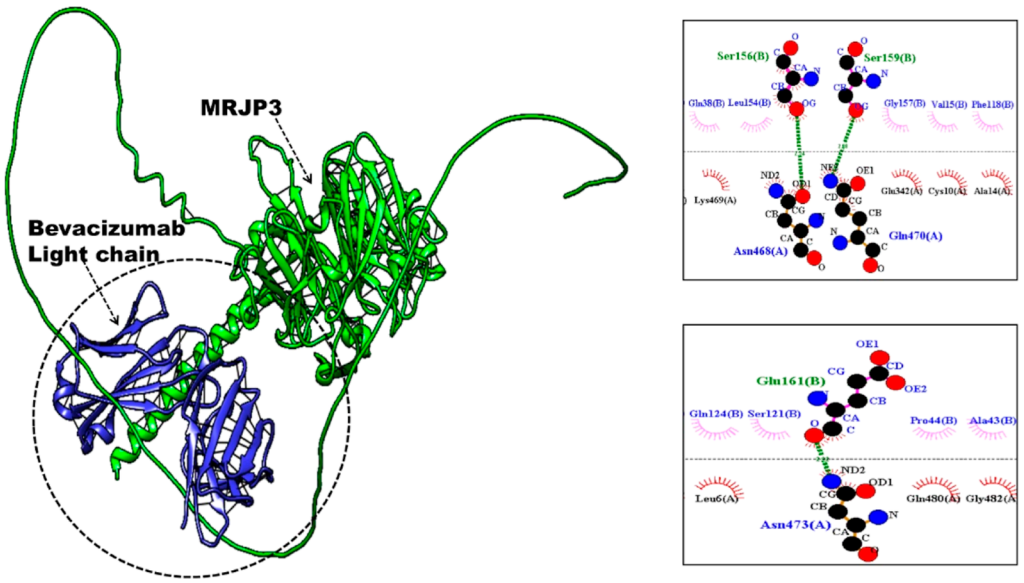

Figure 6. Protein−peptide based molecular residue 3D and 2D interactions of MRJP3 with LC of Bevacizumab.

protein expression analysis and have been confirmed as HUVEC.

2.5. Effect of Bevacizumab, SPH-60, and Its Combination on HUVEC Viability. HUVEC viability for Bevacizumab was 90% at 100 ng/mL, 80.3% at 200 ng/mL, and 68.2% at 400 ng/mL, respectively. Likewise, when treated with SHP-60, HUVEC viability was 93% at 1.6 μM concentration, 85.1% at 3.2 μM concentration, and 75.3% at 6.4 μM concentration, respectively. HUVEC viability at 100 ng/mL Bevacizumab, and 1.6 μM SHP-60 was 81.2%, at 200 ng/mL Bevacizumab, and 3.2 μM SHP-60 was 62.5%, at 400 ng/mL Bevacizumab, and 6.4 μM SHP-60 was 38.2%, respectively. Hence, HUVEC viability ($p < 0.001$) was shown to be dose-dependently reduced (Figure 4). Thus, a concentration of 100 ng/mL Bevacizumab, 1.6 μM SHP-60, and their combination, which exhibited mild inhibition, and this information was used for subsequent experimental work. The cell viability analysis was carried out using MTT assay which is routinely used for this analysis for the HUVEC cell line and other cells[33−35]

2.6. Effect of Bevacizumab, SPH-60, and Its Combination on HUVEC Tube Formation. Sidr honey from the Karak is unique, as it has only two high-molecular-weight proteins. The crude proteins of Sidr honey clearly showed two proteins 60, and 50 kDa (Figure 1b), from which 60 kDa was purified by gel filtration chromatography easily (Figure 1a). This purified SHP-60 was then subjected to investigating its effect on invitro angiogenesis alone as well as in combination with Bevacizumab. As shown in the results (Figure 5), Bevacizumab and SHP-60 combination has been shown to have a synergistic effect in inhibiting in vitro angiogenesis which is quantified by the inhibition of Endo tube formation. HUVEC tube formation induction and inhibition is considered to be one of the most important functional assays that determines the inhibition or induction of in vitro angiogenesis[36−38]

The total tube length was decreased by 32.2% ($p < 0.001$) when treated with bevacizumab. Similarly, the total tube length was decreased by 19% ($p < 0.001$) when treated with SHP-60. The total tube length was considerably decreased by 63.5% ($p < 0.001$) when treated with their combination in comparison with control (Figure 5). These results suggest that bevacizumab and SPH-60 are both effective in inhibiting HUVEC tube formation, and their combination showed more pronounced inhibition. Our findings also showed that at lower concentrations, Bevacizumab (100 ng/mL), SHP-60 (1.6 μM), and their combination had a minimal impact on HUVEC viability and were found to be safe. Our results shows that purified SHP-60 has a prominent effect in inhibiting angiogenesis, which is in accordance with the work as reported by Aryappalli et al. which used crude Manuka honey on angiogenesis using HUVEC as an in vitro model.[39,40] Our results have showed that there is significant inhibition of HUVEC tube formation when treated with SHP-60 and Bevacizumab alone and in combination, which suggests that they will have a synergistic effect on the inhibition of angiogenesis when used in combination.

2.7. Preparation of MRJP3 Protein, Bevacizumab's Light Chain and High Chain 3D Models. With the aid of the mentioned keywords, we found the top-five MRJP proteins, from*Apis mellifera*. It includes MRJP1 (UniProt accession ID: O18330), MRJP2 (UniProt accession ID: O77061), MRJP3 (UniProt accession ID: Q17060), MRJP4 (UniProt accession ID: Q17061), and MRJP5 (UniProt accession ID: O97432). Based on the molecular mass corresponding with the identified electrophoretogram of SHP-60, we selected MRJP3 as our best corresponding protein 3D model for further in silico analysis. The protein was further analyzed; we found 61,661.79 Da molecular weight, with theoretical pI 6.47. The highest amino acid residue present in this sequence was ASN, which was 87 in count, and the lowest count was 5 for TRP. Total number of atoms present were 8461 with a molecular formula of $C_{2639}H_{4126}N_{812}O_{866}S_{18}$. The 3D model taken from AlphaFold database (https://alphafold.ebi.ac.uk/search/text/Q17060) has an overall quality score of 93.30%. The verify3D analysis showed that 81.99% of the residues have averaged 3D-1D score ≥0.1.

The light chain (LC) and heavy chain (HC) of Bevacizumab were also modeled with the aid of SWISS model Web server. The LC of Bevacizumab showed template similarity with PDB

https://doi.org/10.1021/acsomega.3c09736
ACS Omega 2024, 9, 17143−17153

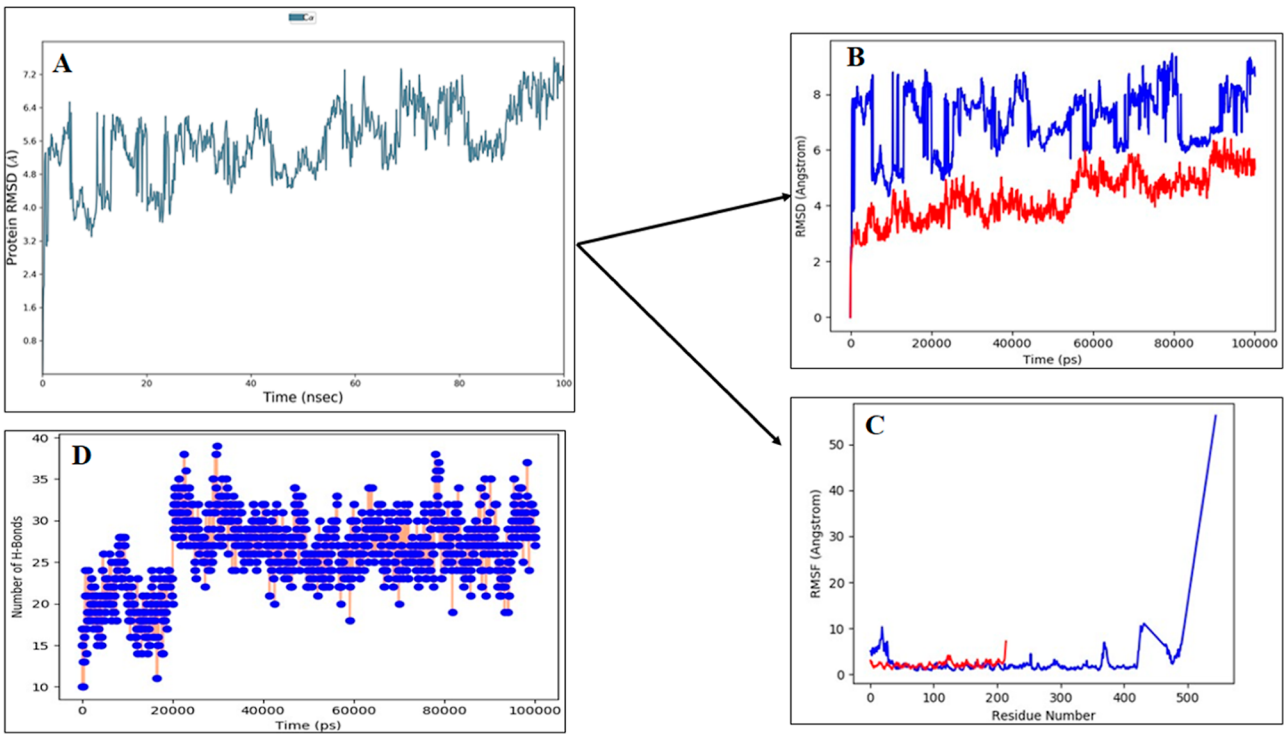

Figure 7. MD simulation analysis of MRJP3 with LC of Bevacizumab. (A,B) MD simulation analysis at 100 ns and 100 000 ps (red color, LC of Bevacizumab; blue color—MRJP3), (C) RMSF plot (red color, LC of Bevacizumab; blue color—MRJP3), and (D) number of hydrogen formation during 100,000 ps MD simulation.

ID 6BFT (A) "structure of Bevacizumab Fab mutant in complex with VEGF", having a sequence similarity of 99.07%. The HC of Bevacizumab showed template similarity with PDB ID 1HZH (B) "crystal structure of the intact human Igg B12 with broad and potent activity against primary Hiv-1 isolates: a template for HIV vaccine design" having a top-ranked sequence similarity of 86.75% compared to the other template based predicted models of the above sequence.

2.8. Protein−Peptide Docking Predictions and Molecular Dynamics Simulations Analysis. The top-ranked model obtained through LZerD docking for investigating the possible bindings of MRJP3 with LC of Bevacizumab was selected on the basis of least GOAP (a knowledge-based potential considering pairwise atoms distance and orientations between atom pairs), DIFIRI (a knowledge-based potential considering pairwise atoms distance), and ITscore (a knowledge-based potential considering pairwise atoms distance) scores, i.e., −94,010.53, −59,165.20, and −29,445.14, respectively (Figure 6). Similarly, the top-ranked model obtained through LZerD docking for investigating the possible bindings of MRJP3 with HC of Bevacizumab was selected based on least GOAP, DIFIRI, and ITscore scores, i.e., −122,452.66, −77,106.86, and −39,041.32, respectively.

Using molecular dynamics (MD), the optimal chemical protein−protein interactions between MRJP3 and bevacizumab's LC and HC were simulated for 100 ns (100 000 ps). Desmond's simulated trajectories were analyzed. Using MD trajectory analysis, the values of the RMSD (root-mean-square deviation) and RMSF (root-mean-square fluctuation) were determined. Figure 7 shows the time-dependent changes in RMSD values for the C-alpha atoms in protein−peptide interactions between MRJP3 with LC of Bevacizumab. The RMSD plot demonstrated that the complex protein with protein−peptide interactions between MRJP3 with LC of Bevacizumab stabilized throughout the provided interval as compared to its interaction with HC of Bevacizumab. The RMSD remains within the range of ∼3.2−6.5 Å throughout the duration of the simulation. The protein−peptide interactions between MRJP3 with LC of Bevacizumab complex got stabilized after 5 ns with reference to RMSD values (Figure 7). Throughout the simulation, the LC peptide's (protein−peptide interactions between MRJP3 with LC of Bevacizumab) RMSD of the protein−peptide interactions between MRJP3 with LC of Bevacizumab was more stable with protein, i.e., ranged between ∼2.5 and 5 Å (100,000 ps) (Figure 7). In this regard, we investigated the molecular interactions of residues between MRJP3 and LC, in which ASN468, GLN470, and ASN473 of MRJP3 showed interaction with SER156, SER159, and GLU161 of LC of Bevacizumab (Figure 7).

Figure 7 shows the RMSF values of the protein−peptide interactions between MRJP3 with the LC of the Bevacizumab complex. We know that residues with greater peaks are found in the *N*- and *C*-terminal zones, or in the areas 420 to 544, based on the MD trajectories. The low RMSF values of the binding site residues of MRJP3 demonstrated the stability of protein−protein interactions between the LC of the Bevacizumab complex and MRJP3 (Figure 7).

The protein−protein interactions have great functional, and structural diversity.[41] To strengthen our findings, we used an in silico approach to validate the protein−protein (SHP-60 with Bevacizumab) molecular interactions, that is, the binding pattern (synergistic effects), to establish the role of SHP-60 with Bevacizumab in managing the challenge of angiogenesis. Protein−protein docking is a computational technique used to predict the three-dimensional structure of a complex formed between both protein molecules and involves simulating the

https://doi.org/10.1021/acsomega.3c09736
ACS Omega 2024, 9, 17143−17153

interactions between the protein and peptide to predict the most energetically favorable or biologically relevant binding mode.[42] Therefore, in the present study, the role of the LC of Bevacizumab in the interaction with MRJP3 (similar in molecular weight to SHP-60) can be predicted as a significant mechanism that could be effective in understanding tumor angiogenesis. This can provide insights into the structural basis of protein−protein interactions and help in understanding the molecular mechanisms underlying various cellular processes.

Protein−protein docking can help in the functional annotation of proteins by predicting their potential binding patterns.[42] MD simulations are computational techniques that model the physical movements of atoms and molecules over time which provide a dynamic view of the interactions between a protein and a peptide or protein.[43,44] MD simulations of protein−peptide docking offer several advantages, including the ability to capture dynamic events, study conformational changes, and provide insights into the thermodynamics of binding. We found significant results during the interactions of the LC of Bevacizumab with MRJP3 (such as SHP-60); hence, it could be postulated that the LC of Bevacizumab offered a more suitable binding pattern with MRJP3, resulting in more significant findings in the conjugation of Bevacizumab with SHP-60 in vitro. We believe that integration of experimental data and computational techniques can enhance the reliability of the findings and can be used for future drug design purpose.

3. CONCLUSIONS

Tumor angiogenesis is essentially important for the progression of cancer and its metastasis, and natural products derived from both plants and animals showing antiangiogenic properties provide an attractive therapeutic approach to combat tumor growth and progression. In the present study, we purified a 60 kDa protein from Sidr honey of the Karak district of KPK (Khyber Pakhtunkhwa) for the first time. We investigated its antioxidant potential, and using HUVEC as an in vitro model of angiogenesis, we showed that Bevacizumab and SHP-60 combination has a significant synergistic effect in inhibiting tumor angiogenesis compared to Bevacizumab alone. These promising results led us to investigate and determine the possible interaction of Bevacizumab with SHP-60, for which we performed in silico analysis. To do this, we used several computational tools to look for potential honey protein sequences that were like SHP-60 available on the Protein Data Bank (PDB), and we selected MRJP3. The LC of Bevacizumab was found to have greater molecular interactions with MRJP3 rather than its HC. Based on this, we have concluded that SHP-60 was attached with Bevacizumab LC in such a way that it significantly inhibits angiogenesis in vitro. These findings suggested that the combination of Bevacizumab and SHP-60 might be an effective therapeutic approach, and further studies in the future can investigate in detail their role in the treatment of malignancies.

4. MATERIALS AND METHODS

4.1. Study's Approval. The study was conducted after approval from the Institutional Review Board (IRB-1673/DUHS/Approval/2020/92 and 2098/DUHS/Approval/2021) of Dow University of Health Sciences. Bevacizumab (Avastin) was purchased commercially. All the experimental research work was carried out at Dow Research Institute of Biotechnology and Biomedical Sciences (DRIBBS), Dow University of Health Sciences.

4.2. Honey Sample Collection. In this study, natural and unprocessed Sidr honey (extracted from the nectar of Lote tree or Ziziphus, commonly called Beri in Urdu) was collected from the Karak district of KPK province of Pakistan. Sidr honey was purchased commercially. The stock solution was serially diluted in the culture medium to get a final concentration of Bevacizumab (100, 200, and 400 ng/mL) and SHP-60 (1.6, 3.2, and 6.4 μM).

4.3. Proteins Extraction from Honey. The honey sample was left overnight at 4 °C after being diluted five times with buffer A (20 mM Tris/HCl and 150 mM NaCl, pH 8.0). Next day, the sample was centrifuged at 8000 rpm to remove particulates like pollens. The collected supernatant was used for the 85% ammonium sulfate precipitation. The sample was centrifuged at 8000 rpm. After discarding the supernatant, the pellet was dissolved in buffer A.[45] The concentration of proteins was measured by Nano Drop Lite Spectrophotometer (Thermo Scientific, USA).

4.4. Gel Filtration Chromatography. The extracted crude honey proteins were subjected to gel filtration chromatography (GFC) on fast protein liquid chromatography (FPLC) utilizing an AKTA pure system (GE Healthcare, Uppsala, Sweden). The gel filtration column Hi-prep 26/60 Sephacryl S-200 column (GE-Healthcare, Uppsala, Sweden) was used. The system was equilibrated with buffer A as the mobile phase. The extracted crude honey proteins dissolved in buffer A were filtered by a 0.22 μm filter (Thermo Scientific, USA) and were applied on to the column with an eluted flow rate of 1 mL/min. The fractions were collected as 2 mL/tube.

4.5. Sodium Dodecyl Sulfate−Polyacrylamide Gel Electrophoresis. Tris/Tricine 12% SDS−PAGE was used to visualize the honey crude proteins and the fractions that were purified using FPLC[46] (Bio-Rad, Mini-PROTEAN Tetra System, USA). For 1 h, the electrophoresis was run at 180 V. Coomassie G-250 (Bio-Rad) was used to stain the gels, and deionized water was used to remove the stain.

4.6. DPPH Radicals Scavenging Activity. DPPH radicals scavenging activity of purified protein from Sidr honey SHP-60 was determined as previously described with few changes.[47,48]

The purified SHP-60 from Sidr honey by using FPLC was collected and dialyzed against water using 3.5 kDa MWCO (molecular weight cut off) dialysis tubing and lyophilized. The lyophilized purified SHP-60 was dissolved in deionized water (at different concentrations of μM). The freshly prepared DPPH in ethanol (0.1 mM) was used for the experiment. In the 96-well plate, SHP-60 solutions of different concentrations (100 μL) and DPPH (100 μL) were combined, and the mixture was incubated for 30 min at room temperature in the dark. Using a microplate reader (Varioskan LUX, Thermo Scientific), and the absorbance was measured at 517 nm against ethanolic DPPH solution as a blank. All samples were used in triplicate. To compute the percent DPPH scavenging activity, the following formula was used

$$\text{DPPH radicals scavenging activity}(\%) = [(A_b - A_s)/A_b] \times 100$$

where A_b and A_s stand for the sample's and blank's respective absorbances.

4.7. HUVEC Cell Culture. The HUVEC cells were resuspended in 10 mL of EBM-2 (Lonza, Walkersville, MD)

https://doi.org/10.1021/acsomega.3c09736
ACS Omega 2024, 9, 17143−17153

supplemented with 10% FBS (Sigma-Aldrich). The T-75 tissue culture flask was used for plating the cells which were then incubated at 37 °C and 5% CO_2. To monitor the cobblestone morphology of the HUVEC, the cells were frequently viewed by using a phase contrast microscope. The culture medium was replaced every other day, until the cells achieved a confluent state. TrypLE Express (Life Technologies) was used to pass the cells.

4.8. Flowcytometry of HUVEC. Molecular characterization of HUVEC was performed through flowcytometry (BD FACS Celesta). Approximately 1×10^6 cells were taken and resuspended in Dulbecco's phosphate buffer saline (DPBS) (Life Technologies). The cells were incubated for 30 min with fluorochrome labeled antibodies CD31, CD105, and CD8 (BD, Pharmingen) against cell surface antigens. CD31 and CD105 were taken as positive and CD8 as negative marker. The data were analyzed using FACS Diva Software 8.0, with unstained cells serving as the control.

4.9. MTT Assay. The viability of HUVEC was evaluated by using the MTT assay (methylthiazolyldiphenyl tetrazolium bromide) (Sigma-Aldrich). HUVEC (15,000 cells/well) were grown in 96-well plate and then incubated for 24 h. The media were changed with fresh culture media supplemented with 5% FBS after 24 h and then treated with different strengths of Bevacizumab (100, 200, and 400 ng/mL), SHP-60 (1.6, 3.2, and 6.4 μM), and the combination of both for 72 h. SHP-60 and bevacizumab-free cells served as the control group. After the desired time, MTT solution (5 mg/mL) was added, and the absorbance at 560 nm was measured with a spectrophotometer.

4.10. Tube Formation Assay. The tube formation assay was used for examining the formation of endotubes for invitro angiogenesis. The 96-well plates were coated with 50 μL/well Geltrex (basement membrane extracted from mouse sarcoma) (Life Technologies) and incubated for 1 h at 37 °C. Once the Geltrex has solidified, HUVEC (20,000 cells/well) were added and then treated with Bevacizumab (100 ng/mL), SHP-60 (1.6 μM) and their combination. Cells without Bevacizumab and SHP-60 were used as a control. After 8−10 h, the endotubes development was examined under a phase contrast microscope. The images were captured at a 10× magnification, and the data were processed using ImageJ software 1.52.

4.11. Statistical Analysis. Every process was carried out in triplicates. The SPSS software 16.0 was used to enter the data. The data were shown as mean ± SD. The control and treatment groups were compared using an ANOVA and Tukey's post hoc test. P value < 0.05 was set as the significant cutoff.

4.12. Selection of SHP-60 Gene/Protein Sequences, 3D Models, and Its Structural Validation. With reference to our obtained electrophoresis findings, we selected the possible gene sequences of SHP-60 from the UniProtKb reference protein database[17] (https://www.uniprot.org/). The search criteria for selection of gene/protein sequences were the use of "Major Royal Jelly Protein (MRJP)" and the organism's name "*A. mellifera*" as keywords. We used canonical protein sequence for the MRJP3 protein. Following is the complete header information on MRJP3 protein sequence, indicating its UniProt accession ID. >sp|Q17060|MRJP3_APIME Major royal jelly protein 3 OS = *A. mellifera* OX = 7460 GN = MRJP3 PE = 1 SV = 1. We selected the SHP protein with a molecular weight corresponding to that of our purified protein from Pakistani Sidr honey.

The next strategy was to prioritize complete 3D protein homology with a thorough structural coverage of amino acid residues after a protein sequence had been chosen. Consequently, using the UniProt database (https://alphafold.ebi.ac.uk),[49] the 3D model of the canonical protein-coding gene sequence (MRJP3: major royal jelly protein 3) was obtained from the AlphaFold Protein Structure Database. The lack of a comprehensive 3D protein model in the Protein Data Bank (PDB)[50] led to the adoption of this strategy. Prior to this, we used the PDB database to do protein BLAST (Basic Local Alignment Search Tool) research.[51]

We selected a 3D model with full coverage (amino acid length of 544) from the canonical sequence of major royal jelly protein 3 (MRJP3) since the sequence query coverage was less than 70%. Following the selection of a 3D protein model, the protein structure was seen and molecular properties were interactively investigated using UCSF Chimera.[52] The PDB structure of MRJP3 was optimized for energy minimization using DeepView/Switzerland-PdbViewer.[53] Using an ERRAT quality factor, Ramachandran plot, Prosa-web (https://prosa.services.came.sbg.ac.at/prosa.php), and the residual properties of the generated model, the PROCHECK stereochemical assessment was used to validate the model. Using the Ramachandran plot, the dihedral angles φ against ψ of potential amino acid conformations in the protein structure were also examined. The likely structural errors and z-scores were ascertained using the structure validation server (SAVES; https://saves.mbi.ucla.edu/). Probable residue characteristics, side chain parameters, chi−chi plot analysis, *G*-factor, and planar group analysis were all determined using the SAVES (Structure Validation Server: https://saves.mbi.ucla.edu/) web server.[54]

4.13. Retrieval of Bevacizumab Peptide Sequences and Its Homology Modeling. As a monoclonal antibody, the drug with the generic name "Bevacizumab", which targets vascular endothelial growth factor and is used to treat several cancer types in conjunction with antineoplastic medicines, comprised light as well as heavy chain protein sequences.[55] Therefore, we separately downloaded both sequences from the DrugBank database (https://go.drugbank.com/) with accession number "DB00112".[56] The SWISS-Model tool was used to predict the homology models of both the HC and LC of bevacizumab[57] using a template-based model selection strategy. The PDB structures of both models were selected based on their higher sequence similarity with alignment and coverage compared to the PDB repository-based template.

4.14. Protein−Protein Docking Prediction and MD Simulations Analysis. The local 3D Zernike descriptor-based protein docking (LZerD) algorithm was used to compute the protein−protein (MRJP3-LC and HC of Bevacizumab) molecular docking interactions.[42] With PDB input files, LZerD uses two protein structures for docking prediction. This method combines geometric hashing with a soft protein surface representation utilizing 3D Zernike descriptors (based on a mathematical moment expansion of the shape function) to produce docked models of submitted input proteins. LZerD algorithm can quickly search the space of binding poses while tolerating side-chain and subunit flexibility. After that, docking models were clustered with a predefined clustering cutoff of 4.0 Å, surface reduction of 1×10^{-4}. Ultimately, the obtained output was of the rank models based on their rank sum from the DFIRE, GOAP, and ITScore scoring functions. The top model was consistently ranked,

https://doi.org/10.1021/acsomega.3c09736
ACS Omega 2024, 9, 17143−17153

ensuring similar distance and angle features to the experimentally determined protein structures. Finally, structural refinement was not applied to the models to ensure that the structures remained consistent.

Desmond, a software application from Schrödinger LLC, was used to run 100 ns (100,000 ps) of MD simulations. For this, rigid binding assessments of the chosen peptide interactions with the target protein were calculated by using protein−peptide docking in MD simulations. Using Newton's classical equation of motion, MD simulations were performed to forecast the protein−peptide binding status in the physiological environment.[56,58]

The chosen protein−peptide interactions were optimized and reduced using Maestro's Protein Preparation Wizard. There were no steric conflicts, poor contacts, or distorted geometries. The systems were constructed using the System Builder tool, and TIP3P (Intermolecular Interaction Potential 3 Points Transferable), an orthorhombic box with the OPLS_2005 force field, was utilized as the solvent model. Throughout the simulation period, 300 K temperature and 1 atm pressure were utilized to imitate physiological circumstances, while counterions were added to neutralize the models and 0.15 M sodium chloride was added. Trajectories were saved every 100 ps (ps) for inspection, and the stability of protein−peptide interactions was determined by measuring the RMSD over time.[56,58]

AUTHOR INFORMATION

Corresponding Author

Mohsin Wahid − *Dow Research Institute of Biotechnology and Biomedical Sciences, Dow University of Health Sciences, Karachi 74200, Pakistan; Department of Pathology, Dow International Medical College, Dow University of Health Sciences, Karachi 74200, Pakistan;* orcid.org/0000-0002-1939-6565; Email: mohsin.wahid@duhs.edu.pk

Authors

Meshal Nazeer − *Dow Research Institute of Biotechnology and Biomedical Sciences, Dow University of Health Sciences, Karachi 74200, Pakistan*

Abdul Qadir − *Dow Research Institute of Biotechnology and Biomedical Sciences, Dow University of Health Sciences, Karachi 74200, Pakistan; Department of Pharmacology, United Medical and Dental College, Karachi 75190, Pakistan;* orcid.org/0000-0002-9133-2558

Muhammad Bilal Azmi − *Department of Biochemistry, Dow Medical College, Dow University of Health Sciences, Karachi 74200, Pakistan;* orcid.org/0000-0001-8320-4479

Complete contact information is available at: https://pubs.acs.org/10.1021/acsomega.3c09736

Author Contributions

M.W. conceptualized, designed, and supervised the study and experimental work and did the final review and approval of the manuscript. M.N. performed the experiments for isolation of protein from the honey including HPLC, FPLC, and SDS page and wrote the manuscript. A.Q. performed the experiments involving HUVEC culture, flowcytometry, MTT assay, and tube formation and wrote the manuscript. M.B.A. performed the in silico analysis and wrote the manuscript.

Funding

None. The study was self-funded.

Notes

The authors declare no competing financial interest.

REFERENCES

(1) Porcza, L. M.; Simms, C.; Chopra, M. Honey and Cancer: Current Status and Future Directions. *Diseases* **2016**, *4*, 30.

(2) Chan-Zapata, I.; Segura-Campos, M. R. Honey and its protein components: Effects in the cancer immunology. *J. Food Biochem.* **2021**, *45*, No. e13613.

(3) G Vallianou, N.; Gounari, P.; Skourtis, A.; Panagos, J.; Kazazis, C. Honey and its anti-inflammatory, anti-bacterial and anti-oxidant properties. *Gen. Med.* **2014**, *02*, 1−5.

(4) Erejuwa, O. O.; Sulaiman, S. A.; Wahab, M. S. A. Effects of honey and its mechanisms of action on the development and progression of cancer. *Molecules* **2014**, *19*, 2497−2522.

(5) Fernandez-Cabezudo, M. J.; El-Kharrag, R.; Torab, F.; Bashir, G.; George, J. A.; El-Taji, H.; al-Ramadi, B. K. Intravenous administration of manuka honey inhibits tumor growth and improves host survival when used in combination with chemotherapy in a melanoma mouse model. *PLoS One* **2013**, *8*, No. e55993.

(6) Alvarez-Suarez, J. M.; Tulipani, S.; Díaz, D.; Estevez, Y.; Romandini, S.; Giampieri, F.; Damiani, E.; Astolfi, P.; Bompadre, S.; Battino, M. Antioxidant and antimicrobial capacity of several monofloral Cuban honeys and their correlation with color, polyphenol content and other chemical compounds. *Food Chem. Toxicol.* **2010**, *48*, 2490−2499.

(7) Mesri, M.; Birse, C.; Heidbrink, J.; McKinnon, K.; Brand, E.; Bermingham, C. L.; Feild, B.; FitzHugh, W.; He, T.; Ruben, S.; et al. Identification and characterization of angiogenesis targets through proteomic profiling of endothelial cells in human cancer tissues. *PLoS One* **2013**, *8*, No. e78885.

(8) Cosmai, L.; Gallieni, M.; Liguigli, W.; Porta, C. Renal toxicity of anticancer agents targeting vascular endothelial growth factor (VEGF) and its receptors (VEGFRs). *J. Nephrol.* **2017**, *30*, 171−180.

(9) Kim, D. G.; et al. *MAbs*; Taylor & Francis, 2015, pp 1195−1204.

.

(10) Dang, Y.-Z.; Zhang, Y.; Li, J. P.; Hu, J.; Li, W. W.; Li, P.; Wei, L. C.; Shi, M. High VEGFR1/2 expression levels are predictors of poor survival in patients with cervical cancer. *Medicine* **2017**, *96*, No. e5772.

(11) Malik, D.; Tarek, M.; Caceres del Carpio, J.; Ramirez, C.; Boyer, D.; Kenney, M. C.; Kuppermann, B. D. Safety profiles of anti-VEGF drugs: bevacizumab, ranibizumab, aflibercept and ziv-aflibercept on human retinal pigment epithelium cells in culture. *Br. J. Ophthalmol.* **2014**, *98*, i11−i16.

(12) Pittarella, P.; Squarzanti, D. F.; Molinari, C.; Invernizzi, M.; Uberti, F.; Renò, F. NO-dependent proliferation and migration induced by Vitamin D in HUVEC. *J. Steroid Biochem. Mol. Biol.* **2015**, *149*, 35−42.

(13) Brudzynski, K.; Sjaarda, C. P. Colloidal structure of honey and its influence on antibacterial activity. *Compr. Rev. Food Sci. Food Saf.* **2021**, *20*, 2063−2080.

(14) Waheed, M.; Hussain, M. B.; Javed, A.; Mushtaq, Z.; Hassan, S.; Shariati, M. A.; Khan, M. U.; Majeed, M.; Nigam, M.; Mishra, A. P.; et al. Honey and cancer: A mechanistic review. *Clin. Nutr.* **2019**, *38*, 2499−2503.

(15) Won, S.-R.; Li, C.-Y.; Kim, J.-W.; Rhee, H.-I. Immunological characterization of honey major protein and its application. *Food Chem.* **2009**, *113*, 1334−1338.

(16) Di Girolamo, F.; D'Amato, A.; Righetti, P. G. Assessment of the floral origin of honey via proteomic tools. *J. Proteomics* **2012**, *75*, 3688−3693.

(17) Pundir, S.; Martin, M. J.; O'Donovan, C. UniProt protein knowledgebase. *Protein Bioinformatics: From Protein Modifications and Networks to Proteomics*; Springer, 2017; Vol. *1558*, pp 41−55.

(18) Bilikova, K.; Kristof Krakova, T.; Yamaguchi, K.; Yamaguchi, Y. Major royal jelly proteins as markers of authenticity and quality of honey / Glavni proteini matične mliječi kao markeri izvornosti i kakvoće meda. *Arh. Hig. Rada Toksikol.* **2015**, *66*, 259−267.

(19) Šimúth, J.; Bíliková, K.; Kováčová, E.; Kuzmová, Z.; Schroder, W. Immunochemical approach to detection of adulteration in honey: physiologically active royal jelly protein stimulating TNF-α release is a regular component of honey. *J. Agric. Food Chem.* **2004**, *52*, 2154−2158.
(20) Albert, Š.; Klaudiny, J.; Šimuth, J. Newly discovered features of the updated sequence of royal jelly protein RJP571; longer repetitive region on C-terminus and homology to Drosophila melanogaster yellow protein. *J. Apic. Res.* **1996**, *35*, 63−68.
(21) Fukuda, M.; Kobayashi, K.; Hirono, Y.; Miyagawa, M.; Ishida, T.; Ejiogu, E. C.; Sawai, M.; Pinkerton, K. E.; Takeuchi, M. Jungle honey enhances immune function and antitumor activity. *J. Evidence-Based Complementary Altern. Med.* **2011**, *2011*, 1−8.
(22) Tonks, A. J.; Dudley, E.; Porter, N. G.; Parton, J.; Brazier, J.; Smith, E. L.; Tonks, A. A 5.8-kDa component of manuka honey stimulates immune cells via TLR4. *J. Leukoc. Biol.* **2007**, *82*, 1147−1155.
(23) Majtan, J.; Kumar, P.; Majtan, T.; Walls, A. F.; Klaudiny, J. Effect of honey and its major royal jelly protein 1 on cytokine and MMP-9 mRNA transcripts in human keratinocytes. *Exp. Dermatol.* **2010**, *19*, e73−e79.
(24) Gannabathula, S.; Krissansen, G. W.; Skinner, M.; Steinhorn, G.; Schlothauer, R. Honeybee apisimin and plant arabinogalactans in honey costimulate monocytes. *Food Chem.* **2015**, *168*, 34−40.
(25) Gannabathula, S.; Skinner, M. A.; Rosendale, D.; Greenwood, J. M.; Mutukumira, A. N.; Steinhorn, G.; Stephens, J.; Krissansen, G. W.; Schlothauer, R. C. Arabinogalactan proteins contribute to the immunostimulatory properties of New Zealand honeys. *Immunopharmacol. Immunotoxicol.* **2012**, *34*, 598−607.
(26) Cianciosi, D.; Forbes-Hernández, T.; Afrin, S.; Gasparrini, M.; Reboredo-Rodriguez, P.; Manna, P.; Zhang, J.; Bravo Lamas, L.; Martínez Flórez, S.; Agudo Toyos, P.; et al. Phenolic compounds in honey and their associated health benefits: A review. *Molecules* **2018**, *23*, 2322.
(27) Chua, L. S.; Lee, J. Y.; Chan, G. F. Characterization of the proteins in honey. *Anal. Lett.* **2015**, *48*, 697−709.
(28) Meo, S. A.; Al-Asiri, S. A.; Mahesar, A. L.; Ansari, M. J. Role of honey in modern medicine. *Saudi J. Biol. Sci.* **2017**, *24*, 975−978.
(29) Khalil, M. I.; Moniruzzaman, M.; Boukraâ, L.; Benhanifia, M.; Islam, M. A.; Islam, M. N.; Sulaiman, S. A.; Gan, S. H. Physicochemical and antioxidant properties of Algerian honey. *Molecules* **2012**, *17*, 11199−11215.
(30) Qadir, A.; Wahid, M.; Asif, M.; Roome, T. Synergistic effect of bevacizumab and celecoxib on angiogenesis in vitro using human umbilical vein endothelial cells. *Int. J. Clin. Pharmacol. Ther.* **2020**, *58*, 696−702.
(31) Heiss, M.; Hellström, M.; Kalén, M.; May, T.; Weber, H.; Hecker, M.; Augustin, H. G.; Korff, T. Endothelial cell spheroids as a versatile tool to study angiogenesis in vitro. *FASEB J.* **2015**, *29*, 3076−3084.
(32) Ponce, M. L. *Angiogenesis protocols*; Springer, 2009, pp 183−188.
(33) Motahari, R.; Boshagh, M. A.; Moghimi, S.; Peytam, F.; Hasanvand, Z.; Oghabi Bakhshaiesh, T.; Foroumadi, R.; Bijanzadeh, H.; Firoozpour, L.; Khalaj, A.; et al. Design, synthesis and evaluation of novel tetrahydropyridothienopyrimidin-ureas as cytotoxic and anti-angiogenic agents. *Sci. Rep.* **2022**, *12*, 9683.
(34) Jiao, K.; Su, P.; Li, Y. FGFR2 modulates the Akt/Nrf2/ARE signaling pathway to improve angiotensin II-induced hypertension-related endothelial dysfunction. *Clin. Exp. Hypertens.* **2023**, *45*, 2208777.
(35) Peng, K.; Jiang, P.; Du, Y.; Zeng, D.; Zhao, J.; Li, M.; Xia, C.; Xie, Z.; Wu, J. Oxidized low-density lipoprotein accelerates the injury of endothelial cells via circ-USP36/miR-98−5p/VCAM1 axis. *IUBMB Life* **2021**, *73*, 177−187.
(36) Guo, L.; Chen, Y.; Feng, X.; Sun, D.; Sun, J.; Mou, S.; Zhao, K.; An, R. Oxidative stress-induced endothelial cells-derived exosomes accelerate skin flap survival through Lnc NEAT1-mediated promotion of endothelial progenitor cell function. *Stem Cell Res. Ther.* **2022**, *13*, 325.
(37) Yi, K.; Yang, Y.; Yuan, Y.; Xiang, Y.; Zhou, S. Impaired Autophagy Causes Severe Corneal Neovascularization. *Cells* **2022**, *11*, 3895.
(38) Wang, R.; Ma, Y.; Zhan, S.; Zhang, G.; Cao, L.; Zhang, X.; Shi, T.; Chen, W. B7-H3 promotes colorectal cancer angiogenesis through activating the NF-κB pathway to induce VEGFA expression. *Cell Death Dis.* **2020**, *11*, 55.
(39) Liu, Y.; Tian, H.; Blobe, G. C.; Theuer, C. P.; Hurwitz, H. I.; Nixon, A. B. Effects of the combination of TRC105 and bevacizumab on endothelial cell biology. *Invest. New Drugs* **2014**, *32*, 851−859.
(40) Aryappalli, P.; Al-Qubaisi, S. S.; Attoub, S.; George, J. A.; Arafat, K.; Ramadi, K. B.; Mohamed, Y. A.; Al-Dhaheri, M. M.; Al-Sbiei, A.; Fernandez-Cabezudo, M. J.; et al. The IL-6/STAT3 signaling pathway is an early target of manuka honey-induced suppression of human breast cancer cells. *Front. Oncol.* **2017**, *7*, 167.
(41) Nooren, I. M.; Thornton, J. M. NEW EMBO MEMBER'S REVIEW: Diversity of protein-protein interactions. *EMBO J.* **2003**, *22*, 3486−3492.
(42) Christoffer, C.; Bharadwaj, V.; Luu, R.; Kihara, D. LZerD protein-protein docking webserver enhanced with de novo structure prediction. *Front. Mol. Biosci.* **2021**, *8*, 724947.
(43) Shukla, R.; Tripathi, T. Molecular dynamics simulation in drug discovery: opportunities and challenges. *Innovations and Implementations of Computer Aided Drug Discovery Strategies in Rational Drug Design*; Springer Nature, 2021; pp 295−− 316.
(44) Wang, J.; Alekseenko, A.; Kozakov, D.; Miao, Y. Improved modeling of peptide-protein binding through global docking and accelerated molecular dynamics simulations. *Front. Mol. Biosci.* **2019**, *6*, 112.
(45) Bocian, A.; Buczkowicz, J.; Jaromin, M.; Hus, K. K.; Legáth, J. An effective method of isolating honey proteins. *Molecules* **2019**, *24*, 2399.
(46) Schägger, H. Tricine−sds-page. *Nat. Protoc.* **2006**, *1*, 16−22.
(47) Arise, A. K.; Alashi, A. M.; Nwachukwu, I. D.; Ijabadeniyi, O. A.; Aluko, R. E.; Amonsou, E. O. Antioxidant activities of bambara groundnut (Vigna subterranea) protein hydrolysates and their membrane ultrafiltration fractions. *Food Funct.* **2016**, *7*, 2431−2437.
(48) Alzahrani, M. A. J.; Perera, C. O.; Hemar, Y. Production of bioactive proteins and peptides from the diatom Nitzschia laevis and comparison of their in vitro antioxidant activities with those from Spirulina platensis and Chlorella vulgaris. *Int. J. Food Sci. Technol.* **2018**, *53*, 676−682.
(49) Varadi, M.; Anyango, S.; Deshpande, M.; Nair, S.; Natassia, C.; Yordanova, G.; Yuan, D.; Stroe, O.; Wood, G.; Laydon, A.; et al. AlphaFold Protein Structure Database: massively expanding the structural coverage of protein-sequence space with high-accuracy models. *Nucleic acids Res.* **2022**, *50*, D439−D444.
(50) Goodsell, D. S.; Zardecki, C.; Di Costanzo, L.; Duarte, J. M.; Hudson, B. P.; Persikova, I.; Segura, J.; Shao, C.; Voigt, M.; Westbrook, J. D.; et al. RCSB Protein Data Bank: Enabling biomedical research and drug discovery. *Protein Sci.* **2020**, *29*, 52−65.
(51) Samal, K. C.; Sahoo, J. P.; Behera, L.; Dash, T. Understanding the BLAST (Basic local alignment search tool) Program and a step-by-step guide for its use in life science research. *Bhartiya Krishi Anusandhan Patrika* **2021**, *36*, 55−61.
(52) Pettersen, E. F.; Goddard, T. D.; Huang, C. C.; Meng, E. C.; Couch, G. S.; Croll, T. I.; Morris, J. H.; Ferrin, T. E. UCSF ChimeraX: Structure visualization for researchers, educators, and developers. *Protein Sci.* **2021**, *30*, 70−82.
(53) Guex, N.; Peitsch, M. C.; Schwede, T. Automated comparative protein structure modeling with SWISS-MODEL and Swiss-PdbViewer: A historical perspective. *Electrophoresis* **2009**, *30*, S162−S173.
(54) Singh, D. B.; Pathak, R. K. *Bioinformatics: methods and applications*; Academic Press, 2021.
(55) Silvestre, A. L. P.; Oshiro-Júnior, J. A.; Garcia, C.; Turco, B. O.; da Silva Leite, J. M.; de Lima Damasceno, B. P. G.; Soares, J. C. M.;

https://doi.org/10.1021/acsomega.3c09736
ACS Omega 2024, 9, 17143−17153

Chorilli, M. Monoclonal antibodies carried in drug delivery nanosystems as a strategy for cancer treatment. *Curr. Med. Chem.* **2020**, *28*, 401−418.
(56) Kandeel, M.; Iqbal, M. N.; Ali, I.; Malik, S.; Malik, A.; Sehgal, S. A. Comprehensive in silico analyses of flavonoids elucidating the drug properties against kidney disease by targeting AIM2. *PLoS One* **2023**, *18*, No. e0285965.
(57) Bienert, S.; Waterhouse, A.; de Beer, T.; Tauriello, G.; Studer, G.; Bordoli, L.; Schwede, T. The SWISS-MODEL Repository—new features and functionality. *Nucleic acids Res.* **2017**, *45*, D313−D319.
(58) Malik, A.; Iqbal, M. N.; Ashraf, S.; Khan, M. S.; Shahzadi, S.; Shafique, M. F.; Sajid, Z.; Sajid, M.; Sehgal, S. A. In silico elucidation of potential drug targets against oxygenase domain of Human eNOS Dysfunction. *PLoS One* **2023**, *18*, No. e0284993.

https://doi.org/10.1021/acsomega.3c09736
ACS Omega 2024, 9, 17143−17153